Linear Regression–based Signal Strength Modeling using Real-World Data

Jáchym Herynek   Martin Zoula   Jan Faigl

***Abstract*— This work presents an efficient method for radio signal strength estimation motivated by mobile ground robot deployments. While machine-learning approaches can avoid the need for empirical material parameters, the computational cost of advanced methods, such as deep learning, can be impractical for robotics planning tasks requiring thousands of queries. Therefore, we propose a linear signal strength prediction model whose parameters are learned from real-world data. The method is validated on communication datasets collected by two autonomous ground robots in an industrial facility using two different communication links. The model accounts for obstacle types and their positions relative to the transmitter and receiver by decomposing the signal path into longitudinal segments and sampling lateral lanes. An ablation study is performed to quantify the impact of explicitly accounting for obstacles and terrain. The reported empirical evaluation supports the method's feasibility, and results show that for $90\,\%$ of test samples, the prediction error is below $9\,\mathrm{dB}$.**

***Index Terms*— Connection availability Ground robots communication Communication prediction**

I. Introduction

Sharing information is critical for efficient coordination in multi-robot deployments, such as multi-robot exploration [1]. Communication availability within the mission area is an important component of maintaining communication between the robots and between the robots and the mission control. Hence, the field of communication-aware robotics [2], [3] merges the reasoning about spatial and temporal communication quality with mission-specific problems, such as search [4], data delivery [5], radio station deployment [6], exploration [7], [8], or reconnection [9], to name a few.

Highly accurate methods for predicting signal availability exist [2]; however, they can be computationally expensive for complex multi-robot planning tasks, where communication availability must be queried thousands of times. Therefore, we propose a generalization of the linear model [10] that accounts for additional details about the obstacles, while preserving the model's linear complexity. For a linear model, the estimation consists of constructing the feature vector and performing a single scalar multiplication. It is a highly desirable model property for planning scenarios because, for example, multi-agent communication-constrained path-planning [11] requires determining communication accessibility at every node expansion.

The authors are with the Faculty of Electrical Engineering, Czech Technical University, Technická 2, 166 27 Prague, Czechia. {herynjac, zoulamar, faiglj}@fel.cvut.cz

The presented research was supported by the Ministry of Education, Youth and Sports of the Czech Republic (MEYS) under Project No. LUABA24064. The work of M. Zoula was funded by the Czech Science Foundation (GAČR) under research Project No. 25-17779M.

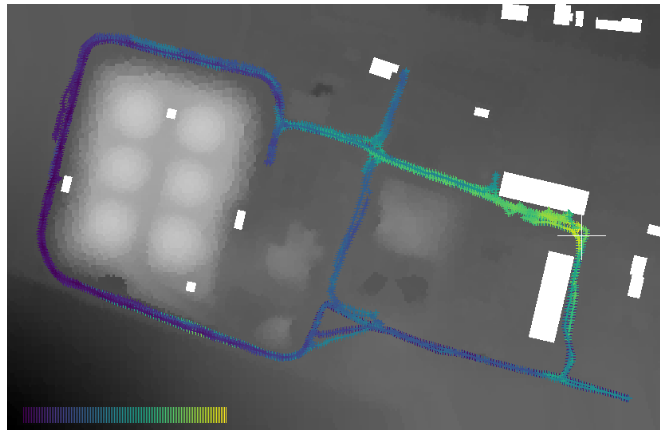

Fig. 1. Visualization of the collected signal strength measurements. Each data point corresponds to a single measurement, where a darker color means a worse signal. The cross shows the location of the base station. Underlying the gray-scale data points is an elevation map with buildings shown in white.

The proposed model has been trained on real-world data, depicted in Fig. 1, gathered using two autonomous ground robotic platforms (see Fig. 3). Based on the empirical evaluation presented herein, the proposed method achieves a significant improvement over the linear model in [10], reducing the median error on the dataset from $5.27\,\mathrm{dB}$ to $3.2\,\mathrm{dB}$.

The rest of the paper is organized as follows. The following section summarizes prior work on signal strength estimation and simulation, along with a brief overview of the selected linear baseline method [10]. The proposed method is presented in Section III and a description of the collected training data is provided in Section IV. The evaluation results, including the ablation study, are presented in Section V. The paper concludes with a summary of the method and the achieved results in Section VI.

II. Related Work

Exploiting earlier foundational results on signal predictability [12], contemporary research in the area already calls for holistic approaches that unite both aspects under a common mission-solving framework [2], [13]. However, feeding such frameworks suitable inputs about the signal (communication) availability or quality remains an open question. As electromagnetic numerical solvers are computationally expensive for on-board use, ray tracing [14] or vector parabolic equation techniques [15] ease the burden. Besides, contemporary robotic equipment does not support rapid, detailed environmental sensing, including material properties such as permittivity, permeability, surface roughness, and moisture, which are significant influences on signal-quality modeling.

That is why surrogate methods and simplifying assumptions are sought. For example, in the subterranean domain, sampling tunnel geometry features enables extrapolating the learned models to areas that have been seen but not yet visited. The work of Clark et al. [16] evaluated line-of-sight conditions, obstacle shadowing, reflection, and diffraction along the signal path and used them to train a neural-network-based predictor, achieving a mean absolute error of $7.28\,\mathrm{dB}$. On the other hand, regression based on Gaussian processes enables precise statistical prediction in and between already visited areas [7]. A hybrid approach was proposed in our previous work [17]. Although the subterranean domain enables the exploitation of advanced waveguide patterns [18] or the automation of predictions via ray tracing [19], recent practical deployments still rely on human decision-making in communication awareness [20], [21]. In aerial robotics, communication directivity [22], urban structures [14], or even the Doppler effect [23] are of interest. Machine learning techniques proved helpful in the signal quality modeling task [24].

As our work concerns ground rovers, we list the most relevant papers we are aware of to date. Weather conditions affect signal strength, and therefore mission conditions need to be taken into account [25]. Recently, Diller et al. [26] proposed a support vector regression technique to infer the expected retransmission count. Local environment features were used in the inference—the straight distance, the shortest obstacle-free distance, the ratio of the two distances, and the number of occupied and unknown nearby map cells. However, their selected regression value remains hard to compare against. Egi et al. [27] used the YOLOv5 network to predict the signal strength from satellite imagery, achieving an estimation error of approximately $3.95\,\%$. Santra et al. [28] predict signal strength from a precise height map of the target environment, considering the free space path loss, reflections in the 2nd Fresnel zone, and the diffraction in the 1st Fresnel zone. The result is verified on an emulated extra-terrestrial exploration scenario.

As an accurate prediction of the signal requires detailed information about the environment, most approaches require some degree of simplifying assumptions. Recently, Ethier et al. [10] proposed a long-range signal strength model that relies on only a few features. Their simplest implementation estimates the path loss as

$$A\log_{10}(f) + B\log_{10}(d) + C \tag{1}$$

where d is the distance between the two points, and f is the frequency, and the parameters A, B, and C are estimated from a real-world dataset. Their work also proposes using more features, namely, terrain depth and clutter depth. It also offers more complex machine-learning-based estimators, which achieve mean errors of $7.26\,\mathrm{dB}$ on the dataset, with points ranging from $0\,\mathrm{m}$ to $30\,\mathrm{km}$ apart. Notably, though, the linear regression model is not much worse than their other, more complex approaches. Therefore, the model is found suitable to fulfill our needs motivated by robotics planning. However, we aim to account for obstacles and their spatial influence on signal propagation; hence, the proposed generalization is presented in the following section.

III. Method

The proposed signal strength modeling is based on the linear regression model [10]. Instead of a single linear model, we generalized the idea into an ensemble of linear models using spatial sampling of the signal path into n_{lon} longitudinal segments and n_{lat} laterally sampled lanes (see Fig. 2) as

$$RSSI = \sum_{i=0}^{n_{\mathrm{lon}}} D_i \log\left(d/n_{\mathrm{lon}}\right) + \left(\sum_{j=0}^{n_{\mathrm{lat}}}\sum_{k=0}^{n_o} F_{ijk}\log\left(f_{ijk}\right)\right) + C. \tag{2}$$

The individual features are denoted f_{ij}, d is the distance between the transmitter and receiver, and D_i, F_{ijk}, and C denote the optimized parameters. The number of the accounted longitudinal segments and lateral lanes is n_{lon} and n_{lat}, respectively. The number of distinct obstacle types is n_o.

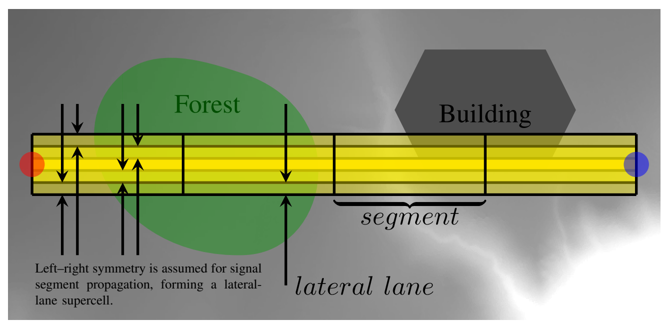

Fig. 2. Illustration of the segmentation of the path between the transmitter and the receiver into a grid. Red and blue disks represent the transmitter and the receiver, respectively. The grid between them visualizes the longitudinal segments and lateral lanes. Each cell on the grid has one feature for each obstacle type. The lanes around the central lane are considered in pairs, assuming that left- and right-handed environmental features have the same effect on signal transmission. The elevation map is shown in shades of gray underlying the grid.

An important factor to consider is the position of the obstacle relative to the transmitter and receiver. It is done by dividing the traveled path into a given number of equal-length **longitudinal segments**. The number of segments n_{lon} is fixed for all data points, meaning that the length of the longitudinal segment is the same within a feature vector, but it varies between individual data points depending on the transmitter-receiver distance d. The setup of longitudinal segments and lateral lanes is further referred to as **grid** or grid density.

The further proposed generalization of [10] accounts for the vicinity of the direct connection path of the transmitter and receiver. We proposed lateral sampling into n_{lat} lanes to differentiate features between small and large obstacles, which can have a greater effect on signal availability. In all reported results, the lateral lane width is set to $1\ \mathrm{meter}$.

Importantly, the proposed lateral lanes are assumed to be symmetric. Each lane, except for the central lane, is paired with its counterpart at the same distance on the opposite side of the path. Such a left–right pair is treated as a single super-cell with twice the area of a regular cell. As a result, n_{lat} is equal to half the lane count, and the five illustrated lanes in Fig. 2 correspond to $n_{\text{lat}} = 3$. The rationale behind this design is as follows.

Although it can be expected that some rays deviate from the direct path, without ray tracing and a detailed environment model, it is not possible to determine whether the deviation is more likely to be left- or right-handed. Therefore, the proposed model assumes that the environmental properties on both sides (left and right) of the direct transmitter-receiver path have the same effect on signal propagation.

Each segment in the grid has a feature for each considered obstacle type. The overall path loss is thus computed as the sum over all segments and lanes. The model is capable of accounting for different types of obstacles, provided they are easily identifiable, for example, by segmentation of the aerial imagery. In the collected dataset, two obstacle types are dominant: terrain (a small hill between the robot and the base station) and buildings. However, any obstacle can be accounted for and incorporated into the model. For each obstacle, the total path length of that obstacle in its segment is determined (by sampling the map data along the segment), and the sum of those lengths forms the feature value, while the position is encoded in the segment. For the non-center lanes, we determine the proportions of the left and right lanes covered by the obstacle, then compute the average coverage across the left and right lanes. We obtain the feature value by multiplying the proportion by the segment length.

The total number of parameters of the model is given as $n_{\text{lon}}(1 + n_{\text{lat}} n_o) + 1$; see (2). The example depicted in Fig. 2 has 41 features, $n_o = 3$ (forest, building, terrain), $n_{\text{lon}} = 4$, and $n_{\text{lat}} = 3$.

The feature vector consists of a sequence of $\log$ terms, where each element other than the distance is the proportion of an obstacle type in a given cell. One needs to construct the feature vector for those two points to estimate the communication strength between two points, and substitute the features into (2), which is a scalar multiplication of the feature vector with the parameter vector. Hence, the computation complexity can be bounded by $O\left(n_{\text{lon}} n_{\text{lat}} n_o\right)$.

IV. Data Gathering

Open geospatial data from OpenStreetMap [29] is used to identify obstacles on the map. It provides a wide variety of labels that can be queried individually, allowing us to pick out whatever is in the area that could affect signal strength. Besides, accurate elevation data are obtained from [30].

The rest of the section is dedicated to the descriptions of the robotic platforms used and the communication devices in the following part. In Section IV-B, the data collection methodology and deployment area are described.

Fig. 3. On the left, the base station with GNSS receiver and communication hardware. On the right, the wheeled robot Husky A200 with a GNSS receiver providing localization data and the communication hardware measuring signal strength. The orange disks show the location of the Mesh-FSK Flood communication receiver, and the blue dot shows the location of the Mesh-LTE receiver.

A. Utilized Platforms and Devices

A stationary base station and two mobile wheeled robots, Husky A200 by Clearpath Robotics, were used to collect signal strength data. The equipment is depicted in Fig. 3 The mobile robots were equipped with a hardware and software solution for localization and communication with the base station.

Both the base station and the robots are equipped with a Global Navigation Satellite System (GNSS) receiver, which provides **localization** data. The GNSS setup consists of the Septentrio mosaic-go module and AS-ANT3B-CAL-L antenna. Furthermore, the base station improves the robot localization by providing Real-Time Kinematic (RTK) corrections. The GNSS and communication devices are connected to an on-board computer of the Intel NUC class, which manages the data collection using ROS Noetic on Ubuntu 20.04.

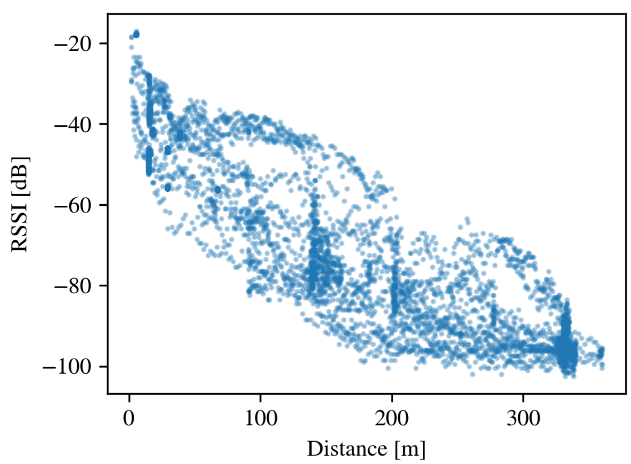

Fig. 4. Distribution of the Mesh-LTE signal strength according to the distance of the mobile receiver to the transmitter at the base station.

The base station and robots are each equipped with a pair of distinct **communication devices**, yielding two separate datasets. The first communication link is established by the Mobilicom MCU-30 Lite, operating at $2480\,\mathrm{MHz}$ with a transmission power of $23\,\mathrm{dBm}$ [31]. The devices form a Hybrid Mesh-LTE network (one base station and two mobile units) and are hereafter referred to as Mesh-LTE. A distribution of signal strength by distance from the base station is depicted in Fig. 4.

The second communication link uses the RFM69HW transceiver at $868\,\mathrm{MHz}$ with a power of $20\,\mathrm{dBm}$. Due to the modulation scheme and flood-fill routing [8] used, the link is referred to as Mesh-FSK Flood. Although both communication channels support mesh networking, they were operated in a point-to-point configuration during the data-gathering campaign.

B. Collection Methodology and Area

The mobile robots collected signal strength data as they traversed a predefined area while receiving signals from the stationary base station. The robotic platforms are localized using GNSS; therefore, the location estimates are combined with signal-strength data to create a unified dataset in which each data point consists of the transmitter and receiver locations and signal strength. These data points are then placed in the elevation and obstacle maps to compute the feature vector.

The data were gathered in an outdoor area roughly $200\ \mathrm{meter} \times 400\ \mathrm{meter}$ in size, which featured different obstacle types: terrain differences (see the elevation visualization in Fig. 1) and buildings. All data was gathered on the same day under consistent weather conditions. The datasets gathered consist of 5000 data points for the Mesh LTE and $14\,000$ for the Mesh-FSK Flood.

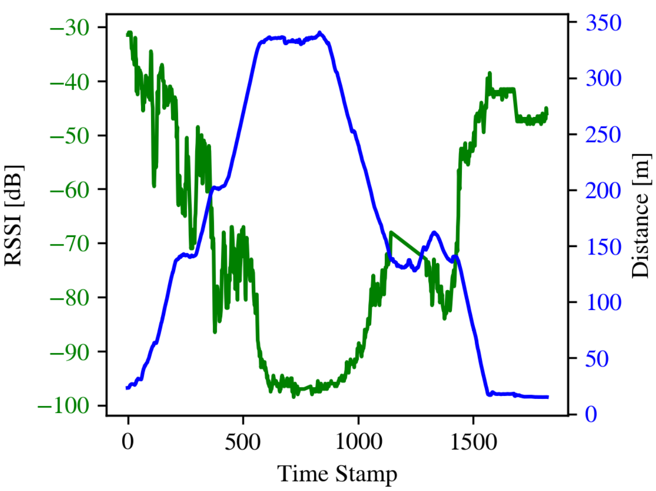

Fig. 5. Mesh LTE signal strength waveform for a single round-trip, plotted against the distance from the base station.

The robots traversed the data collection paths multiple times, as shown in Fig. 4. For most of the trajectory, the base station was on higher ground, with a small hill obstructing line-of-sight (LOS) to the receiver. Additionally, at multiple points, buildings, trees, and other obstacles blocked the signal path. The distances in the dataset range from $0\,\mathrm{m}$ to $400\,\mathrm{m}$, with the signal strength ranging between $-20\,\mathrm{dB}$ and $-100\,\mathrm{dB}$. A signal strength during one such trip around the area is depicted in Fig. 5.

We are aware that the area did not allow for much variation in paths, which is a shortcoming to be addressed in our future experimental deployments.

V. Results

The proposed method, based on an ensemble of linear models, has been evaluated using the collected data for the Mesh-LTE and Mesh-FSK Flood communication links. For $n_{\mathrm{lon}} = n_{\mathrm{lat}} = 1$, the method corresponds to the former approach [10], in which the authors consider an elevation model and account for the portion of the direct communication path segment that passes through the obstacles. However, we consider two types of obstacles: the buildings and the terrain. Hence, for the most straightforward setup, the number of features is 4. The proposed method allows finer grid sampling based on the number of segments and lanes.

TABLE I
MEDIAN ERROR DEPENDING ON THE GRID SIZES (DIAGONAL OF FIG. 6).

	Median error [dB]							
$n_{\mathrm{lon}}/n_{\mathrm{lat}}$	1/1	2/2	3/3	4/4	5/5	6/6	7/7	8/8
Feature count	4	11	22	37	56	79	106	137
Mesh-LTE	5.27	5.06	4.75	4.70	4.26	3.95	3.44	3.20
Mesh-FSK Flood	4.53	4.37	4.26	4.14	3.74	3.64	3.53	3.57

Numerical values of the median error depending on the grid size are depicted in Table I. The complete ablation matrix for increasing grid size for the Mesh-LTE is presented in Fig. 6. The results support the superior performance of the

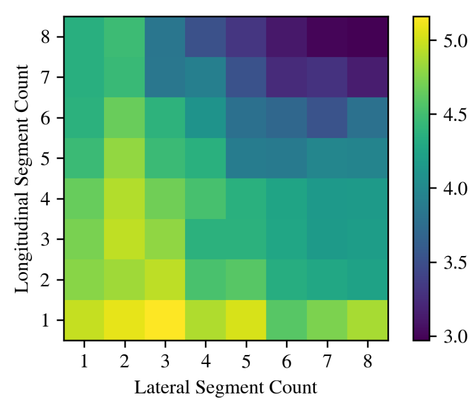

Fig. 6. Lateral and longitudinal segment count influence. The value shown is the mean error on the entire dataset for the Mesh-LTE signal data.

proposed model, which provides more accurate predictions with an increased grid size. The proposed method performs significantly better than [10], with a median error of around $5\,\mathrm{dB}$. Increasing the grid density improves median error values by about $40\,\%$. The distribution of the error is shown in Fig. 7, with the median and 90th percentile values highlighted.

The terrain-feature ablation study is depicted in Table II. The results suggest that including obstacles significantly

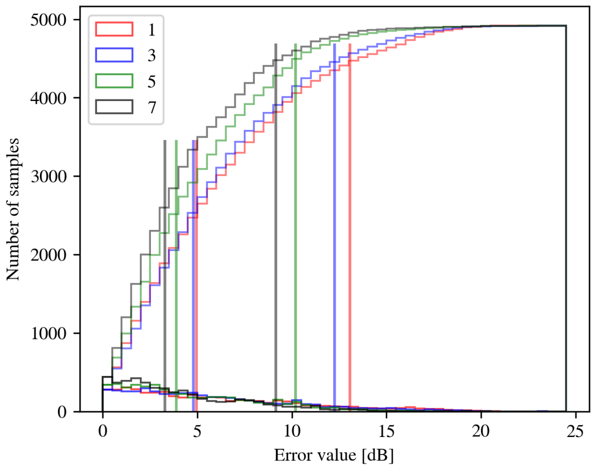

Fig. 7. Error distribution for predictors with $n_{\text{lon}} = n_{\text{lat}}$ and $n_{\text{lon}}, n_{\text{lat}} \in \{1, 3, 5, 7\}$, for selected estimators. Vertical lines correspond to the median and the 90th percentile. Labels correspond to the longitudinal segments n_{lon} and lateral lanes n_{lat}. For each predictor, both the histogram and the cumulative histogram are shown.

TABLE II
MEDIAN ERROR FOR DIFFERENT TERRAIN-FEATURE ABLATIONS.

$n_{\text{lon}}/n_{\text{lat}}$	All	w/o Buildings	w/o Terrain	w/o Either
		Mesh LTE		
1/1	4.96	5.26	7.29	7.23
3/3	4.80	5.00	6.58	6.68
5/5	3.89	4.56	5.07	6.20
7/7	3.30	4.56	3.96	5.61
		Mesh-FSK Flood		
1/1	4.54	4.67	4.58	4.69
3/3	4.26	4.60	4.40	4.72
5/5	3.74	4.24	3.85	4.45
7/7	3.53	4.22	3.65	4.32

improved the estimator's performance, reducing the median error by $30\,\%$ to $50\,\%$, depending on the grid density.

A. Computational Requirements

Although the computational cost of inferring the signal strength prediction is negligible due to the linear nature of the model (2), increasing the grid density increases the computational demands of the learning phase. The number of features n is given as $n = n_{\text{lon}} \times (1 + n_{\text{lat}} \times n_o)$, where n_{lon} and n_{lat} are the numbers of the longitudinal segments and lateral lanes, respectively, and n_o denotes the number of distinguished obstacles in the environment. Thus, the model has 137 parameters for the most dense parameter settings, for which feature vector construction and training become computationally non-negligible.

In particular, for C++ implementation and Mesh-LTE dataset with 5000 data points that runs on AMD Ryzen 7 7840U with already processed OSM data, the computation of the features from the data takes about $300\,\text{ms}$ for the feature vector of the size $n = 137$, and $140\,\text{ms}$ for the model with $n = 22$ parameters.

The computation time of the model estimation itself is negligible for both the C++ implementation using GNU Scientific Library (GSL) [32], as well as for the Python implementation using NumPy [33] (the one shown in the results).

B. Comments on Mesh-FSK Flood Results

The signal of the second communication link based on Mesh-FSK Flood is slightly weaker than for the Mesh-LTE, see Table I. The lower-powered signal was prevented from getting any connection behind the small hill (on the left of the map in Fig. 1). The Mesh-FSK Flood signal also had a much higher sampling frequency than Mesh-LTE, meaning more data was collected, even though no signal was received in parts of the map. The total number of individual data points is about $13\,000$.

Because the signal is weaker, there is very little data with obstacles in the path, which is likely part of the reason why changing the grid density results in a more minor increase in accuracy than with the LTE-Mesh signal. Even though the data points with obstacles were relatively underrepresented, the inclusion of those obstacles still achieved noticeable improvement, but only $5\,\%$ to $20\,\%$, as can be seen in Table II. Similarly to the Mesh-LTE estimator, the improvement from considering more obstacle types is more pronounced when the grid is denser.

VI. CONCLUSION

The paper presents a regression model based on an ensemble of linear models for estimating the received signal strength from map information. The proposed model is evaluated using model training on real-world data collected by two autonomous robotic platforms operating in an industrial environment. The dataset contained terrain obstacles, man-made objects, and two different communication links, both of which achieved similar accuracy with the proposed regression model. The results, albeit simple, support the model's accuracy and achieve median error rates in units of dB on the training dataset. The model's simplicity is its main feature. It can be of significant importance, for example, in planning tasks, where the expected communication strength between two locations is queried many times during the computation.

ACKNOWLEDGMENTS

The work of M. Zoula was funded by the Czech Science Foundation (GAČR) under research Project no. 25-17779M. The authors would like to thank Martin Škarytka for robot preparation and Rudolf Jakub Szadkowski for his active involvement in data collection.

REFERENCES

[1] J. Bayer and J. Faigl, "Decentralized multi-robot exploration under low-bandwidth communications," *Autonomous Robots*, vol. 50, no. 7, 2026. doi: 10.1007/s10514-025-10234-3

[2] J. Gielis, A. Shankar, and A. Prorok, "A critical review of communications in multi-robot systems," *Current Robotics Reports*, vol. 3, no. 4, pp. 213–225, Dec. 2022. doi: 10.1007/s43154-022-00090-9

[3] D. B. Licea, G. Silano, M. Ghogho, and M. Saska, "Communications-aware robotics: Challenges and opportunities," in *International Conference on Unmanned Aircraft Systems (ICUAS)*, 2023, pp. 366–371. doi: 10.1109/ICUAS57906.2023.10155882

[4] A. Bhatt, M. K. Corra, F. Merlo, P. KrisshnaKumar, and S. Chowdhury, "Experimental setup and software pipeline to evaluate optimization based autonomous multi-robot search algorithms," *CoRR*, 2025. doi: 10.48550/arXiv.2506.16710

[5] D. Palma, A. Zolich, Y. Jiang, and T. A. Johansen, "Unmanned aerial vehicles as data mules: An experimental assessment," *IEEE Access*, vol. 5, pp. 24 716–24 726, 2017. doi: 10.1109/ACCESS.2017.2769658

[6] M. Zoula and J. Faigl, "Wireless communication infrastructure building for mobile robot search and inspection missions," in *IEEE International Conference on Robotics and Automation (ICRA)*, 2024, pp. 5970–5976. doi: 10.1109/ICRA57147.2024.10611561

[7] F. Amigoni, J. Banfi, N. Basilico, I. Rekleitis, and A. Quattrini Li, "Online update of communication maps for exploring multirobot systems under connectivity constraints," in *Distributed Autonomous Robotic Systems*, N. Correll, M. Schwager, and M. Otte, Eds. Springer International Publishing, 2019, pp. 513–526. doi: 10.1007/978-3-030-05816-6_36

[8] J. Bayer, P. Čížek, and J. Faigl, "Autonomous Multi-Robot Exploration with Ground Vehicles in DARPA Subterranean Challenge Finals," *Field Robotics*, vol. 3, pp. 266–300, 2023. doi: 10.55417/fr.2023008

[9] A. Muralidharan and Y. Mostofi, "Communication-aware robotics: Exploiting motion for communication," *Annual Review of Control, Robotics, and Autonomous Systems*, vol. 4, no. Volume 4, 2021, pp. 115–139, 2021. doi: 10.1146/annurev-control-071420-080708

[10] J. Ethier and M. Châteauvert, "Machine learning-based path loss modeling with simplified features," *IEEE Antennas and Wireless Propagation Letters*, vol. 23, no. 11, pp. 3997–4001, 2024. doi: 10.1109/LAWP.2024.3388253

[11] H.-D. Bui, E. Plaku, and G. J. Stein, "Multi-agent pathfinding under team-connected communication constraint via adaptive path expansion and dynamic leading," *CoRR*, 2026. doi: 10.48550/arXiv.2501.02770

[12] M. Malmirchegini and Y. Mostofi, "On the spatial predictability of communication channels," *IEEE Transactions on Wireless Communications*, vol. 11, no. 3, pp. 964–978, 2012. doi: 10.1109/TWC.2012.012712.101835

[13] D. Bonilla Licea, M. Ghogho, and M. Saska, "When robotics meets wireless communications: An introductory tutorial," *Proceedings of the IEEE*, vol. 112, no. 2, pp. 140–177, 2024. doi: 10.1109/JPROC.2024.3380373

[14] H. An, K. Guan, W. Li, J. Zhang, D. He, F. Zhu, and L. Chen, "Measurement and ray-tracing for uav air-to-air channel modeling," in *IEEE International Conference on Electronic Information and Communication Technology (ICEICT)*, 2022, pp. 415–420. doi: 10.1109/ICEICT55736.2022.9908966

[15] X. Zhang and C. D. Sarris, "Vector parabolic equation modeling of wireless propagation in tunnels with statistically rough surface walls," in *2018 International Applied Computational Electromagnetics Society Symposium (ACES)*, 2018, pp. 1–2. doi: 10.23919/ROPACES.2018.8364122

[16] L. Clark, J. A. Edlund, M. S. Net, T. S. Vaquero, and A. akbar Agha-mohammadi, "Propem-l: Radio propagation environment modeling and learning for communication-aware multi-robot exploration," *CoRR*, 2022. doi: 10.48550/arXiv.2205.01267

[17] M. Zoula, M. Prágr, and J. Faigl, "On building communication maps in subterranean environments," in *Modelling and Simulation for Autonomous Systems*, J. Mazal, A. Fagiolini, P. Vasik, and M. Turi, Eds., 2021, pp. 15–28. doi: 10.1007/978-3-030-70740-8_2

[18] D. Tardioli, L. Riazuelo, D. Sicignano, C. Rizzo, F. Lera, J. L. Villarroel, and L. Montano, "Ground robotics in tunnels: Keys and lessons learned after 10 years of research and experiments," *Journal of Field Robotics*, vol. 36, no. 6, pp. 1074–1101, 2019. doi: 10.1002/rob.21871

[19] M. D. Bedford, A. Hrovat, G. Kennedy, T. Javornik, and P. Foster, "Modeling microwave propagation in natural caves using lidar and ray tracing," *IEEE Transactions on Antennas and Propagation*, vol. 68, no. 5, pp. 3878–3888, 2020. doi: 10.1109/TAP.2019.2957969

[20] T. Rouček, M. Pecka, P. Čížek, T. Petříček, J. Bayer, V. Šalanský, T. Azayev, D. Heřt, M. Petrlík, T. Báča, V. Spurný, V. Krátký, P. Petráček, D. Baril, M. Vaidis, V. Kubelka, F. Pomerleau, J. Faigl, K. Zimmermann, M. Saska, T. Svoboda, and T. Krajník, "System for Multi-Robotic Exploration of Underground Environments CTU-CRAS-NORLAB in the DARPA Subterranean Challenge," *Field Robotics*, vol. 2, pp. 1779–1818, 2022. doi: 10.55417/fr.2022055

[21] M. Tranzatto, T. Miki, M. Dharmadhikari, L. Bernreiter, M. Kulkarni, F. Mascarich, O. Andersson, S. Khattak, M. Hutter, R. Siegwart, and K. Alexis, "Cerberus in the darpa subterranean challenge," *Science Robotics*, vol. 7, no. 66, p. eabp9742, 2022. doi: 10.1126/scirobotics.abp9742

[22] D. B. Licea, H. El Hammouti, G. Silano, and M. Saska, "Harnessing the potential of omnidirectional multi-rotor aerial vehicles in cooperative jamming against eavesdropping," in *IEEE Global Communications Conference*, 2024, pp. 2052–2058. doi: 10.1109/GLOBECOM52923.2024.10901802

[23] B. Hua, H. Ni, Q. Zhu, C.-X. Wang, T. Zhou, K. Mao, J. Bao, and X. Zhang, "Channel modeling for uav-to-ground communications with posture variation and fuselage scattering effect," *IEEE Transactions on Communications*, vol. 71, no. 5, pp. 3103–3116, 2023. doi: 10.1109/TCOMM.2023.3255900

[24] Z. Becvar, J. Plachy, P. Mach, A. Nikolov, and D. Gesbert, "Machine learning for channel quality prediction: From concept to experimental validation," *IEEE Transactions on Wireless Communications*, vol. 23, no. 10, pp. 14 605–14 619, 2024. doi: 10.1109/TWC.2024.3417532

[25] E. Goldoni, P. Savazzi, L. Favalli, and A. Vizziello, "Correlation between weather and signal strength in lorawan networks: An extensive dataset," *Computer Networks*, vol. 202, p. 108627, 2022. doi: 10.1016/j.comnet.2021.108627

[26] J. Diller, J. G. Rogers, N. T. Dantam, and Q. Han, "Communication mapping for robot teams," *IEEE Transactions on Field Robotics*, vol. 2, pp. 288–307, 2025. doi: 10.1109/TFR.2025.3568794

[27] Y. Egi and E. Eyceyurt, "Classified 3d mapping and deep learning-aided signal power estimation architecture for the deployment of wireless communication systems," *EURASIP Journal on Wireless Communications and Networking*, vol. 2022, no. 1, p. 107, 2022. doi: 10.1186/s13638-022-02188-2

[28] S. Santra, L. B. Paet, M. Laine, K. Yoshida, and E. Staudinger, "Experimental validation of deterministic radio propagation model developed for communication-aware path planning," in *IEEE International Conference on Automation Science and Engineering (CASE)*, 2021, pp. 1241–1246. doi: 10.1109/CASE49439.2021.9551653

[29] OpenStreetMap contributors, "Planet dump retrieved from https://planet.osm.org ," https://www.openstreetmap.org, 2017.

[30] Český zeměměřičský úřad, "Geoportál ČÚZK." [Online]. Available: https://geoportal.cuzk.cz/ [Accessed: 2026-02-05]

[31] "Mobilicom MCU-30 Lite." [Online]. Available: https://mobilicom.com/products/mcu-30-lite/ [Accessed: 2026-02-05]

[32] M. Galassi, J. Davies, J. Theiler, B. Gough, G. Jungman, M. Booth, and F. Rossi, *GNU Scientific Library Reference Manual*, 3rd ed., B. Gough, Ed. Bristol, UK: Network Theory Ltd., 2009. [Online]. Available: https://www.gnu.org/software/gsl/ [Accessed: 2026-02-05]

[33] C. R. Harris, K. J. Millman, S. J. van der Walt, R. Gommers, P. Virtanen, D. Cournapeau, E. Wieser, J. Taylor, S. Berg, N. J. Smith, R. Kern, M. Picus, S. Hoyer, M. H. van Kerkwijk, M. Brett, A. Haldane, J. F. del Río, M. Wiebe, P. Peterson, P. Gérard-Marchant, K. Sheppard, T. Reddy, W. Weckesser, H. Abbasi, C. Gohlke, and T. E. Oliphant, "Array programming with NumPy," *Nature*, vol. 585, no. 7825, pp. 357–362, 2020. doi: 10.1038/s41586-020-2649-2